

Electron-Transfer Oxidation of 9-Substituted 10-Methyl-9,10-dihydroacridines. Cleavage of the C-H vs C-C Bond of the Radical Cations

Shunichi Fukuzumi,^{*,†} Yoshihiro Tokuda,[†] Toshiaki Kitano,[†] Toshihiko Okamoto,[†] and Junzo Otera^{*,‡}

Contribution from the Department of Applied Chemistry, Faculty of Engineering, Osaka University, Suita, Osaka 565, Japan, and Department of Applied Chemistry, Okayama University of Science, Ridai-cho, Okayama 700, Japan

Received April 20, 1993*

Abstract: Electron-transfer oxidation of various 9-substituted 10-methyl-9,10-dihydroacridines (AcrHR) by $\text{Fe}(\text{ClO}_4)_3$ and $[\text{Fe}(\text{phen})_3](\text{PF}_6)_3$ (phen = 1,10-phenanthroline) results in cleavage of the C(9)-H or C(9)-C bond of $\text{AcrHR}^{+\bullet}$ depending on the substituent R. Transient electronic absorption spectra as well as electron spin resonance (ESR) spectra of $\text{AcrHR}^{+\bullet}$ have been detected by using a stopped-flow spectrophotometer and a rapid mixing flow ESR technique, respectively. The hyperfine splitting constants (hfs) are determined by comparing the observed ESR spectra with those from the computer simulation. Comparison of the hfs values with those expected from the molecular orbital calculations indicates the structural change of $\text{AcrHR}^{+\bullet}$ with the substituent R, which is reflected in the selectivity of the C-H vs C-C bond cleavage of $\text{AcrHR}^{+\bullet}$ depending on the substituent R. The decay rates of $\text{AcrHR}^{+\bullet}$ obey the mixture of first-order and second-order kinetics due to the deprotonation (or the C-C bond cleavage) and disproportionation reactions, respectively. Both the first-order and bimolecular second-order decay rate constants of $\text{AcrHR}^{+\bullet}$ are reported. The first-order decay rate constant for the deprotonation of $\text{AcrHR}^{+\bullet}$ by the C-H bond cleavage decreases with the substitution in order R = primary > secondary > tertiary alkyl groups, while the first-order decay due to the C-C bond cleavage becomes dominant with tertiary alkyl groups. The one-electron oxidation potentials of various AcrHR have been determined directly by applying fast cyclic voltammetry. The $\text{p}K_a$ values of $\text{AcrHR}^{+\bullet}$ (R = H and Me) have also been evaluated by analyzing the dependence of the first-order deprotonation rate constants on the concentrations of HClO_4 .

Introduction

The biological importance of dihydronicotinamide adenine dinucleotide (NADH) used as an electron source has attracted considerable interest in electron-transfer reactions from NADH and its analogs to various one-electron oxidants, in which the radical cations of NADH and analogs should be formed.¹⁻⁴ However, no ESR spectra of NADH or analogs have so far been reported because of the instability, although the transient electronic spectra of NADH and analogs have recently been reported.⁵⁻⁷ Such instability of radical cations of NADH analogs

has precluded the direct determination of the fundamental properties for the electron-transfer oxidation, such as the one-electron oxidation potentials, the structure, and the $\text{p}K_a$ values of radical cations. Recently Savéant et al.⁸ have succeeded in determining the one-electron oxidation potential (E°_{ox}) of an NADH analog, 10-methyl-9,10-dihydroacridine (AcrH_2), by applying fast cyclic voltammetry as $E^{\circ}_{\text{ox}} = 0.86 \text{ V}$ (vs SCE), which agrees well with the value estimated previously by us on the basis of the Marcus theory of electron transfer.^{9,10} It is certainly desired to obtain more data concerning fundamental properties of radical cations of NADH analogs by the direct detection of the transient species.

This study reports the first observation of ESR spectra of transient radical cations of NADH analogs formed in electron-transfer oxidation with Fe^{3+} or Cu^{2+} in acetonitrile by applying a rapid-mixing ESR technique.¹¹ 9-Substituted 10-methyl-9,10-dihydroacridines (AcrHR) are used as NADH analogs. The dihydroacridines are stable toward acids,¹² while NADH and ordinary NADH analogs are known to decompose in the presence

[†] Osaka University.

[‡] Okayama University of Science.

* Abstract published in *Advance ACS Abstracts*, September 1, 1993.

- (1) (a) Kosower, E. M. In *Free Radicals in Biology*; Pryor, W. A., Ed.; Academic Press: New York, 1976; Vol. II, p 1. (b) Bruice, T. C. In *Progress in Bioorganic Chemistry*; Kaiser, F. T., Kezdy, F. J., Eds.; Wiley: New York, 1976; Vol. IV, p 1. (c) Kill, R. J.; Widdowson, D. A. In *Bioorganic Chemistry*; van Tamelen, E. E., Ed.; Academic Press: New York, 1978; Vol. IV, p 239. (d) Sigman, D. S.; Hajdu, J.; Creighton, D. J. *Bioorganic Chemistry*; van Tamelen, E. E., Ed.; Academic Press: New York, 1978; Vol. IV, p 385. (e) Yasui, S.; Ohno, A. *Bioorg. Chem.* 1986, 14, 70.
- (2) (a) Powell, M. F.; Wu, J. C.; Bruice, T. C. *J. Am. Chem. Soc.* 1984, 106, 3850. (b) Shinha, A.; Bruice, T. C. *J. Am. Chem. Soc.* 1984, 106, 7291. (c) Okamoto, T.; Ohno, A.; Oka, S. *J. Chem. Soc., Chem. Commun.* 1977, 181. (d) Okamoto, T.; Ohno, A.; Oka, S. *Bull. Chem. Soc. Jpn.* 1980, 53, 330. (e) Fukuzumi, S.; Kondo, Y.; Tanaka, T. *J. Chem. Soc., Perkin Trans. 2* 1984, 673. (f) Fukuzumi, S.; Mochizuki, S.; Tanaka, T. *J. Am. Chem. Soc.* 1989, 111, 1497. (g) Fukuzumi, S.; Kitano, T.; Mochida, K. *J. Am. Chem. Soc.* 1990, 112, 3246. (h) Fukuzumi, S.; Mochizuki, S.; Tanaka, T. *Inorg. Chem.* 1990, 29, 653. (i) Fukuzumi, S.; Yorisue, T. *J. Chem. Soc., Perkin Trans. 2* 1991, 1607. (j) Fukuzumi, S.; Mochizuki, S.; Tanaka, T. *J. Phys. Chem.* 1990, 94, 722. (k) Fukuzumi, S.; Chiba, M. *J. Chem. Soc., Perkin Trans. 2* 1991, 1393.
- (3) Fukuzumi, S.; Tanaka, T. In *Photoinduced Electron Transfer*; Fox, M. A., Chanon, M., Eds.; Elsevier: Amsterdam, 1988; Part C, pp 578-636.
- (4) Fukuzumi, S. *Advances in Electron Transfer Chemistry*; Mariano, P. S., Ed.; JAI Press: Greenwich; Vol. 2, pp 67-175.

- (5) (a) Czochralska, B.; Lindqvist, L. *Chem. Phys. Lett.* 1983, 101, 297. (b) Lindqvist, L.; Czochralska, B.; Grigorov, I. *Chem. Phys. Lett.* 1985, 119, 494.

- (6) (a) Manring, L. E.; Peters, K. S. *J. Am. Chem. Soc.* 1983, 105, 5708. (b) Manring, L. E.; Peters, K. S. *J. Am. Chem. Soc.* 1985, 107, 6452.

- (7) Fukuzumi, S.; Mochizuki, S.; Tanaka, T. *J. Chem. Soc., Dalton Trans.* 1990, 695.

- (8) Hapiot, P.; Moiroux, J.; Savéant, J.-M. *J. Am. Chem. Soc.* 1990, 112, 1337.

- (9) Fukuzumi, S.; Koumitsu, S.; Hironaka, K.; Tanaka, T. *J. Am. Chem. Soc.* 1987, 109, 305.

- (10) Marcus, R. A. *Annu. Rev. Phys. Chem.* 1964, 15, 155.

- (11) A preliminary report has appeared; Fukuzumi, S.; Kitano, T. *Chem. Lett.* 1990, 1275.

- (12) Fukuzumi, S.; Ishikawa, M.; Tanaka, T. *Tetrahedron* 1986, 42, 1021.

of acids.¹³ By changing the alkyl (or phenyl) substituent the reactivity of AcrHR⁺⁺ can be systematically varied and finely tuned to cover a wide range of subtle molecular effects including the electron donor and acid properties. In fact, we have found that the C(9)–H or C(9)–C bond of AcrHR⁺⁺ formed by the electron-transfer oxidation is cleaved to yield 10-methylacridinium ion (AcrH⁺) or 9-alkyl-10-methylacridinium ion (AcrR⁺) and that the selectivity of the C–H vs C–C bond cleavage varies systematically depending on the change in substituent R. The selectivities are compared with the change in the decay rates of AcrHR⁺⁺ which can be readily determined by monitoring the transient absorption spectra of AcrHR⁺⁺ with use of a stopped-flow spectrophotometer. The pK_a values of AcrHR⁺⁺ formed by the electron-transfer oxidation of the acid-stable AcrHR can also be determined from the deprotonation rate constants in the presence of various concentrations of HClO₄ in MeCN.

Experimental Section

Materials. 9,10-Dihydro-10-methylacridine (AcrH₂) was prepared from 10-methylacridinium iodide (AcrH⁺I⁻) by reduction with NaBH₄ in methanol and purified by recrystallization from ethanol.¹⁴ 10-Methylacridinium iodide was prepared by the reaction of acridine with methyl iodide in acetone, and converted to the perchlorate salt (AcrH⁺ClO₄⁻) by the addition of magnesium perchlorate to the iodide salt, and purified by recrystallization from methanol.⁹ The deuterated compound, [9,9'-²H₂]-10-methylacridine (AcrD₂), was prepared from 10-methylacridone by reduction with LiAlD₄,¹⁵ which was obtained from Aldrich. 9,10-Dihydro-10-([²H₃]methyl)acridine (AcrH₂-CD₃) was prepared by NaBH₄ reduction of 10-([²H₃]methyl)acridinium iodide, which was obtained by reaction of acridine with CD₃I in methanol.²¹ 1-Benzyl-1,4-dihydronicotinamide (BNAH) was prepared according to the literature.¹⁶ 9-Alkyl (or phenyl)-9,10-dihydro-10-methylacridine (AcrHR; R = Me, Et, CH₂Ph, Ph) was prepared by the reduction of AcrH⁺I⁻ with the corresponding Grignard reagents (RMgX). Typically a solution of 6 cm³ (4.9 mmol) of MeMgBr (0.82 M in THF) was added dropwise to a suspension of AcrH⁺I⁻ (0.51 g, 1.6 mmol) in CH₂Cl₂ under an atmospheric pressure of nitrogen. After the reaction mixture was stirred for 3 h at room temperature when the color changed from dark orange to pale yellow, an aqueous solution of 5% NaHCO₃ (50 cm³) was added to the mixture. The product was extracted with diethyl ether three times (30 cm³ × 3), and the solvent was evaporated under reduced pressure after drying with MgSO₄. The crude product was recrystallized from H₂O–EtOH–MeCN (yield 76%). AcrHR (R = Prⁱ, Buⁱ, CHPh₂, 1-CH₂C₁₀H₇) was prepared by the photoreduction of AcrH⁺ClO₄⁻ with RCOOH in the presence of NaOH in H₂O–MeCN as reported previously.¹⁷ AcrHR (R = CH₂COOEt, CMe(H)COOEt, and CMe₂COOMe) was prepared by the reduction of AcrH⁺ClO₄⁻ with the corresponding ketene silyl acetal (CH₂=C(OEt)OSiEt₃, CMe(H)=C(OEt)OSiEt₃, and Me₂C=C(OMe)OSiMe₃, respectively).¹⁸

The purity of AcrHR thus obtained was checked by elemental analysis and ¹H NMR spectra. Anal. Calcd for C₁₅H₁₅N (AcrHMe): C, 86.1; H, 7.2; N, 6.7. Found: C, 85.5; H, 7.2; N, 6.6. ¹H NMR (CD₃CN) δ 1.25 (d, 3H), 3.49 (s, 3H), 4.11 (q, 1H), 6.9–7.3 (m, 8H). Anal. Calcd for C₁₆H₁₇N (AcrHEt): C, 86.1; H, 7.7; N, 6.3. Found: C, 86.1; H, 7.7; N, 6.3. ¹H NMR (CD₃CN) δ 0.75 (t, 3H), 1.49 (m, 2H), 3.35 (s, 3H), 3.76 (t, 1H), 6.9–7.2 (m, 8H). Anal. Calcd for C₂₁H₁₉N (AcrHCH₂Ph): C, 88.4; H, 6.7; N, 4.9. Found: C, 88.6; H, 6.7; N, 5.0. ¹H NMR (CD₃CN) δ 2.75 (d, 2H), 3.28 (s, 3H), 4.15 (t, 1H), 6.7–7.3 (m, 13H). Anal. Calcd for C₂₀H₁₇N (AcrHPh): C, 88.5; H, 6.3; N, 5.2.

(13) NADH and the ordinary model compounds decompose in the presence of acids: (a) Johnson, C. C.; Gardner, J. L.; Suelter, C. H.; Metzler, D. E. *Biochemistry* **1963**, *2*, 689. (b) Kim C. S. Y.; Chaykin, S. *Biochemistry*, **1968**, *7*, 2339. (c) van Eikeren, P.; Grier, D. L.; Eliason, J. *J. Am. Chem. Soc.* **1979**, *101*, 7406.

(14) Roberts, R. M. G.; Ostović, D.; Kreevoy, M. M. *Faraday Discuss. Chem. Soc.* **1982**, *74*, 257.

(15) (a) Ostović, D.; Roberts, R. M. G.; Kreevoy, M. M. *J. Am. Chem. Soc.* **1983**, *105*, 7629. (b) Kreevoy, M. M.; Lee, I-S. H. *J. Am. Chem. Soc.* **1984**, *106*, 2550.

(16) (a) Anderson, A. G., Jr.; Berkelhammer, G. *J. Am. Chem. Soc.* **1958**, *80*, 992. (b) Mauzerall, D.; Westheimer, F. H. *J. Am. Chem. Soc.* **1955**, *77*, 2261.

(17) Fukuzumi, S.; Kitano, T.; Tanaka, T. *Chem. Lett.* **1989**, 1231.

(18) Otera, J.; Wakahara, Y.; Kamei, H.; Sato, T.; Nozaki, H.; Fukuzumi, S. *Tetrahedron Lett.* **1991**, *32*, 2405.

Found: C, 88.5; H, 6.3; N, 5.2. ¹H NMR (CD₃CN) δ 3.38 (s, 3H), 5.23 (s, 1H), 6.9–7.3 (m, 13H). Anal. Calcd for C₁₇H₁₉N (AcrHPrⁱ): C, 86.0; H, 8.0; N, 5.9. Found: C, 85.0; H, 7.7; N, 6.0. ¹H NMR (CD₃CN) δ 0.76 (d, 6H), 1.38 (m, 1H), 3.51 (s, 3H), 3.75 (d, 1H), 6.9–7.3 (m, 8H). Anal. Calcd for C₁₈H₂₁N (AcrHBuⁱ): C, 86.0; H, 8.4; N, 5.6. Found: C, 85.4; H, 8.3; N, 5.7. ¹H NMR (CD₃CN) δ 0.78 (s, 9H), 3.42 (s, 3H), 3.72 (s, 1H), 6.9–7.3 (m, 8H). Anal. Calcd for C₂₇H₂₃N (AcrHCH-Ph₂): C, 89.7; H, 6.4; N, 3.9. Found: C, 89.3; H, 6.4; N, 4.0. ¹H NMR (CD₃CN) δ 3.51 (s, 3H), 4.13 (d, 1H), 4.83 (d, 1H), 6.8–7.4 (m, 18H). Anal. Calcd for C₂₅H₂₁N (AcrHCH₂C₁₀H₇): C, 89.5; H, 6.3; N, 4.2. Found: C, 89.2; H, 6.3; N, 4.2. ¹H NMR (CD₃CN) δ 3.30 (d, 2H), 3.42 (s, 3H), 4.36 (t, 1H), 6.8–8.0 (m, 15H). Anal. Calcd for C₁₈H₁₉NO₂ (AcrHCH₂COOEt): C, 76.8; H, 6.8; N, 5.0. Found: C, 76.9; H, 6.8; N, 5.0. ¹H NMR (CD₃CN) δ 1.11 (t, 3H), 2.51 (d, 2H), 3.55 (s, 3H), 4.13 (q, 2H), 4.55 (t, 1H), 6.9–7.4 (m, 8H). Anal. Calcd for C₁₉H₂₁NO₂ (AcrHCHMe(H)COOEt): C, 77.3; H, 7.2; N, 4.7. Found: C, 77.1; H, 7.2; N, 4.7. ¹H NMR (CD₃CN) δ 0.89 (d, 3H), 1.04 (t, 3H), 2.61 (m, 1H), 3.54 (s, 3H), 4.04 (q, 2H), 4.23 (d, 1H), 6.9–7.4 (m, 8H). Anal. Calcd for C₁₉H₂₁NO₂ (AcrHCHMe₂COOEt): C, 77.3; H, 7.2; N, 4.7. Found: C, 76.6; H, 7.2; N, 4.7. ¹H NMR (CD₃CN) δ 0.87 (s, 6H), 3.40 (s, 3H), 3.63 (s, 3H), 4.28 (s, 1H), 6.9–7.4 (m, 8H).

Tris(1,10-phenanthroline)iron(III) hexafluorophosphate, [Fe(phen)₃](PF₆)₃, was prepared by oxidizing a solution of the iron(II) complex with ceric sulfate in an aqueous solution containing H₂SO₄.¹⁹ Iron perchlorate [Fe(ClO₄)₃·9H₂O] and perchloric acid (HClO₄, 70%) were obtained commercially. Acetonitrile used as a solvent was purified and dried by the standard procedure.²⁰

Reaction Procedure. Typically, Fe(ClO₄)₃ (4.0 × 10⁻² M) was added to an NMR tube that contained a CD₃CN solution (0.60 cm³) of AcrHR (4.0 × 10⁻² M) under an atmospheric pressure of argon. The oxidized products of AcrHR were identified as 10-methylacridinium ion (AcrH⁺) and alcohols (ROH) or 9-alkyl-10-methylacridinium ion (AcrR⁺) and H⁺ by comparing their ¹H NMR spectra with those of the authentic samples. The ¹H NMR measurements were performed with Japan Electron Optics JNM-PS-100 (100 MHz) and JNM-GSX-400 (400 MHz) NMR spectrometers. ¹H NMR (CD₃CN): AcrH⁺ClO₄⁻ δ 4.76 (s, 3H), 7.9–8.8 (m, 8H), 9.87 (s, 1H); AcrMe⁺ClO₄⁻ δ 3.48 (s, 3H), 4.74 (s, 3H), 7.9–8.9 (m, 8H); AcrEt⁺ClO₄⁻ δ 1.52 (t, 3H), 3.95 (q, 2H), 4.71 (s, 3H), 7.9–8.9 (m, 8H); AcrPh⁺ClO₄⁻ δ 4.83 (s, 3H), 7.5–8.6 (m, 13H); AcrCH₂Ph⁺ClO₄⁻ δ 4.79 (s, 3H), 5.35 (s, 2H), 7.5–8.9 (m, 13H); AcrCHPh₂⁺ClO₄⁻ δ 4.70 (s, 3H), 5.96 (s, 1H), 7.5–8.9 (m, 18H); Acr(1-CH₂C₁₀H₇)⁺ClO₄⁻ δ 4.80 (s, 3H), 5.72 (s, 2H), 7.5–8.9 (m, 15H); AcrCH₂COOEt⁺ClO₄⁻ δ 1.09 (t, 3H), 2.41 (q, 2H), 4.76 (s, 3H), 5.02 (s, 2H); 7.7–8.7 (m, 8H); AcrCMe(H)COOEt⁺ClO₄⁻ δ 1.20 (t, 3H), 1.93 (d, 3H), 2.59 (q, 2H), 4.74 (s, 3H), 5.49 (q, 1H), 7.7–8.7 (m, 8H).

Kinetic Measurements. Kinetic measurements were performed on a Union RA-103 stopped-flow spectrophotometer at 298 K. Decay of transient radical cations (AcrHR⁺⁺) formed in electron transfer from AcrHR (1.0 × 10⁻⁴ M) to Fe³⁺ (1.5 × 10⁻³ M) or [Fe(phen)₃]³⁺ (5.0 × 10⁻⁴ M) in deaerated MeCN was followed by measuring the disappearance of the absorbance due to AcrHR⁺⁺ in the long-wavelength region (640–710 nm). The effects of HClO₄ on the decay rates of AcrHR⁺⁺ (R = H, Me) formed in electron transfer from AcrHR (1.0 × 10⁻⁴ M) to Fe(ClO₄)₃ (7.5 × 10⁻⁴–5.0 × 10⁻³ M) were examined by monitoring the disappearance of the absorbance due to AcrH₂⁺⁺ and AcrHMe⁺⁺ in the presence of various concentrations of HClO₄ (1.2 × 10⁻²–1.2 × 10⁻¹ M) and H₂O (0.25 M) in deaerated MeCN. The effects of a base (3,5-dichloro-pyridine) on the decay rates of AcrHR⁺⁺ (R = Me, CH₂Ph) formed in electron transfer from AcrHR (1.0 × 10⁻⁴ M) to [Fe(phen)₃]³⁺ (5.0 × 10⁻⁴ M) were examined by monitoring the disappearance of the absorbance due to AcrHR⁺⁺ in the presence of various concentrations of 3,5-dichloropyridine (3.0 × 10⁻³–1.0 × 10⁻² M) in deaerated MeCN. The first-order and second-order decay kinetics were analyzed with an NEC PC computer.

ESR Measurements. The ESR measurements were performed on a JEOL X-band spectrometer (JES-ME-LX). Deaerated MeCN solutions of AcrHR (1.0 × 10⁻³ M) and Fe(ClO₄)₃ (8.5 × 10⁻⁴ M) under an atmospheric pressure of nitrogen were mixed in the capillary cell by using a JEOL JES-SM-1 rapid mixing flow apparatus. The flow rate was 1–2 cm³ s⁻¹. The ESR spectra were recorded under non-saturating microwave power conditions. The magnitude of modulation was chosen to optimize

(19) (a) Ford-Smith, M. H.; Sutin, N. *J. Am. Chem. Soc.* **1961**, *83*, 1830. (b) Fukuzumi, S.; Nishizawa, N.; Tanaka, T. *Bull. Chem. Soc. Jpn.* **1982**, *55*, 3482.

(20) Perrin, D. D.; Armarego, W. L. F.; Perrin, D. R. *Purification of Laboratory Chemicals*; Pergamon Press: Elmsford, 1966.

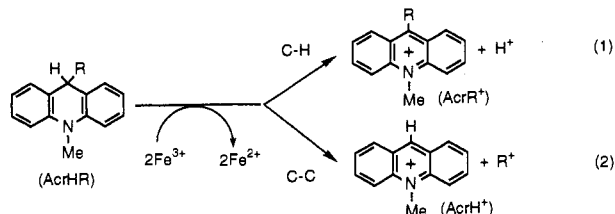
the resolution and the signal-to-noise (S/N) ratio of the observed spectra. The g values and hyperfine splitting constants (hfs) were calibrated by using an Mn^{2+} marker. The simulations of ESR spectra were performed by using an NEC PC computer.

Fast Cyclic Voltammetry. The fast cyclic voltammetry measurements were performed on a Fuso Model HECS 972 potentiostat-galvanostat by using a function generator Fuso Model HECS 980 and a Riken transient memory Model TCFL-8000E. The platinum microelectrode (10 μm i.d.) was obtained from BAS Co., LTD, and it was routinely cleaned by soaking it in concentrated nitric acid, followed by repeated rinsing with water and acetone and drying at 353 K prior to use in order to avoid possible fouling of the electrode surface. The reference electrode was an Ag/0.01 M $AgNO_3$. The cyclic voltammograms were measured with various sweep rates in deaerated MeCN containing 1.0×10^{-1} M Bu_4NClO_4 used as a supporting electrolyte at 298 K.

Theoretical Calculations. The theoretical studies were performed with use of the PM3 molecular orbital method.²¹ The MOPAC program (QCPE No. 455), which was revised as OS/2 Version 5.01 to adapt for the use on a NEC PC computer, was obtained through the Japan Chemistry Program Exchange (JCPE).²² The structural output was recorded by using the MOPC program (JCPE No. P038). The calculations were also performed by using the MOL-GRAH program Ver. 2.8 by Daikin Industries, Ltd. Final geometries and energetics were obtained by optimizing the total molecular energy with respect to all structural variables. The geometries of the radical cations were optimized by using the unrestricted Hartree-Fock (UHF) formalism. The adiabatic ionization potentials (I_a) were calculated as the difference in the heat of formation (ΔH_f) between the radical cation and the corresponding neutral form, when the ΔH_f values of the radical cations were calculated with the UHF-optimized structures by using the half-electron (HE) method.²³

Results and Discussion

Cleavage of the C-H Bond vs the C-C Bond of AcrHR Accompanied by Electron-Transfer Oxidation with Fe^{3+} . When 9-substituted 10-methyl-9,10-dihydroacridine (AcrHR) is oxidized by $Fe(ClO_4)_3$ or $[Fe(phen)_3](PF_6)_3$ in deaerated MeCN, the C(9)-H bond of AcrHR is cleaved to yield 9-alkyl-10-methylacridinium ion ($AcrR^+$) and H^+ (eq 1) or the C(9)-C bond is cleaved to 10-methylacridinium ion ($AcrH^+$) and R^+ (eq 2), depending on the substituent R. The products yields are shown



in Table I. In the case of $R = Me, Et, Ph,$ and CH_2COOEt , the C(9)-H bond of AcrHR is cleaved exclusively to yield $AcrR^+$ selectively (eq 1). In contrast, the C(9)-C bond of AcrHR is cleaved selectively in the case of $R = Bu^+$ and CMe_2COOMe to yield $AcrH^+$ and R^+ . The carbonium ions R^+ formed primarily may react with H_2O contained in MeCN to yield mainly the corresponding alcohols (see Experimental Section). In the case of $R = CH_2Ph, 1-CH_2C_{10}H_7, CMe(H)COOEt, Pr^i,$ and $CHPh_2$, both the C-H and C-C bonds of AcrHR are cleaved to yield the two types of products shown in eqs 1 and 2 (Table I). In the presence of H_2O (2.0 M), the selectivity for the C-H bond cleavage in the $AcrHCH_2Ph-Fe^{3+}$ system increases significantly to yield $AcrCH_2Ph^+$ (88%) as compared to the yield (45%) without the addition of H_2O as shown in Table I.

Transient Electronic and ESR Spectra of $AcrHR^{2+}$. Mixing an acetonitrile (MeCN) solution of $Fe(ClO_4)_3$ with AcrHR in a stopped-flow spectrometer results in an instant appearance of

Table I. Electron-Transfer Oxidation of AcrHR (4.0×10^{-2} M) by $Fe(ClO_4)_3$ and $[Fe(phen)_3](PF_6)_3$ in Deaerated MeCN at 298 K

AcrHR R =	product (yield, %) ^a	
Me	$AcrMe^+$ (100, 100 ^b)	$AcrH^+$ (0, 0 ^b)
Et	$AcrEt^+$ (100)	$AcrH^+$ (0)
Ph	$AcrPh^+$ (100)	$AcrH^+$ (0)
CH_2COOEt	$AcrCH_2COOEt^+$ (100)	$AcrH^+$ (0)
$CMe(H)COOEt$	$AcrCMe(H)COOEt^+$ (77)	$AcrH^+$ (23)
CH_2Ph	$AcrCH_2Ph^+$ (45)	$AcrH^+$ (55)
CH_2Ph	$AcrCH_2Ph^+$ (88) ^c	$AcrH^+$ (12) ^c
Pr^i	$AcrPr^i^+$ (40, 43 ^b)	$AcrH^+$ (60, 57 ^b)
$1-CH_2C_{10}H_7$	$AcrCH_2C_{10}H_7^+$ (17, 35 ^b)	$AcrH^+$ (83, 65 ^b)
$CHPh_2$	$AcrCHPh_2^+$ (25, 20 ^b)	$AcrH^+$ (75, 80 ^b)
Bu^+	$AcrBu^+^+$ (0)	$AcrH^+$ (100)
CMe_2COOMe	$AcrCMe_2COOMe^+$ (0)	$AcrH^+$ (100)

^a In the oxidation by $Fe(ClO_4)_3$ (4.0×10^{-2} M) unless otherwise noted.

^b In the oxidation by $[Fe(phen)_3](PF_6)_3$ (4.0×10^{-2} M). ^c In the presence of 2.0 M H_2O .

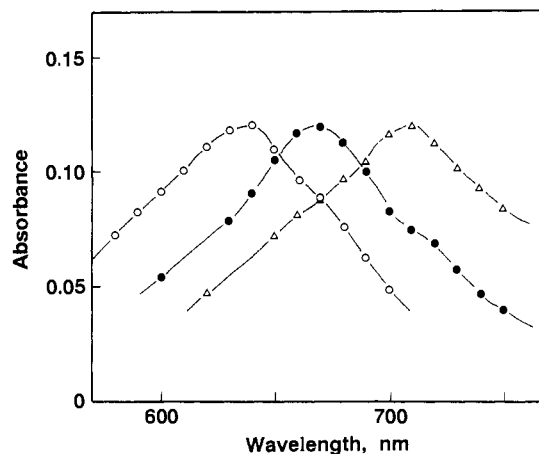


Figure 1. Transient absorption spectra of $AcrHR^{2+}$ formed in the electron-transfer oxidation of AcrHR (1.0×10^{-4} M) by $[Fe(phen)_3](PF_6)_3$ (5.0×10^{-4} M) in deaerated MeCN at 298 K: $R = H$ (O), Et (●), and Bu^+ (Δ).

a new transient absorption band at λ_{max} 640–710 nm depending on the substituent R as shown in Figure 1.⁷ Essentially the same transient spectrum is obtained when the oxidant $Fe(ClO_4)_3$ is replaced by $[Fe(phen)_3]^{3+}$ or $Cu(ClO_4)_2$. Thus, appearance of a new transient absorption band may be ascribed to formation of radical cation $AcrHR^{2+}$ (eq 3). In fact, the ESR spectra are



observed in the electron-transfer oxidation of AcrHR with Fe^{3+} in deaerated MeCN by applying a rapid-mixing ESR technique as shown in Figure 2. The g -values of $AcrHR^{2+}$ with various substituents R are essentially the same as 2.0027, indicating the contribution of spin-orbit coupling due to electron spin at the nitrogen nucleus. The ESR signal decayed rapidly when the flow of the reactant solution was stopped as observed in the transient absorption spectrum. Deuterium substitution at appropriate known sites may permit an experimental verification of the assignment of the observed radical species, since a single deuterium gives a triplet (instead of doublet) hyperfine pattern and the deuterium splitting should decrease by the magnetogyric ratio of proton to deuterium (0.153).²⁴ In fact, deuterium substitution of two hydrogen atoms at the C-9 position of $AcrH_2$ results in drastic changes in the splitting pattern from the spectrum in Figure 2a to that in Figure 2b, where $AcrH_2$ is substituted by 10-methyl-[9,9- $2H_2$]dihydroacridine ($AcrD_2$). The substitution of one hydrogen atom with various alkyl or phenyl groups at the

(21) Stewart, J. J. P. *J. Comput. Chem.* **1989**, *10*, 209, 221.

(22) Toyoda, J. *JCPE News Lett.* **1990**, *2*, 37.

(23) Clark, T. *A Handbook of Computational Chemistry*; Wiley: New York, 1985; p 97.

(24) Wertz, J. E.; Bolton, J. R. *Electron Spin Resonance Elementary Theory and Practical Applications*; McGraw-Hill: New York, 1972.

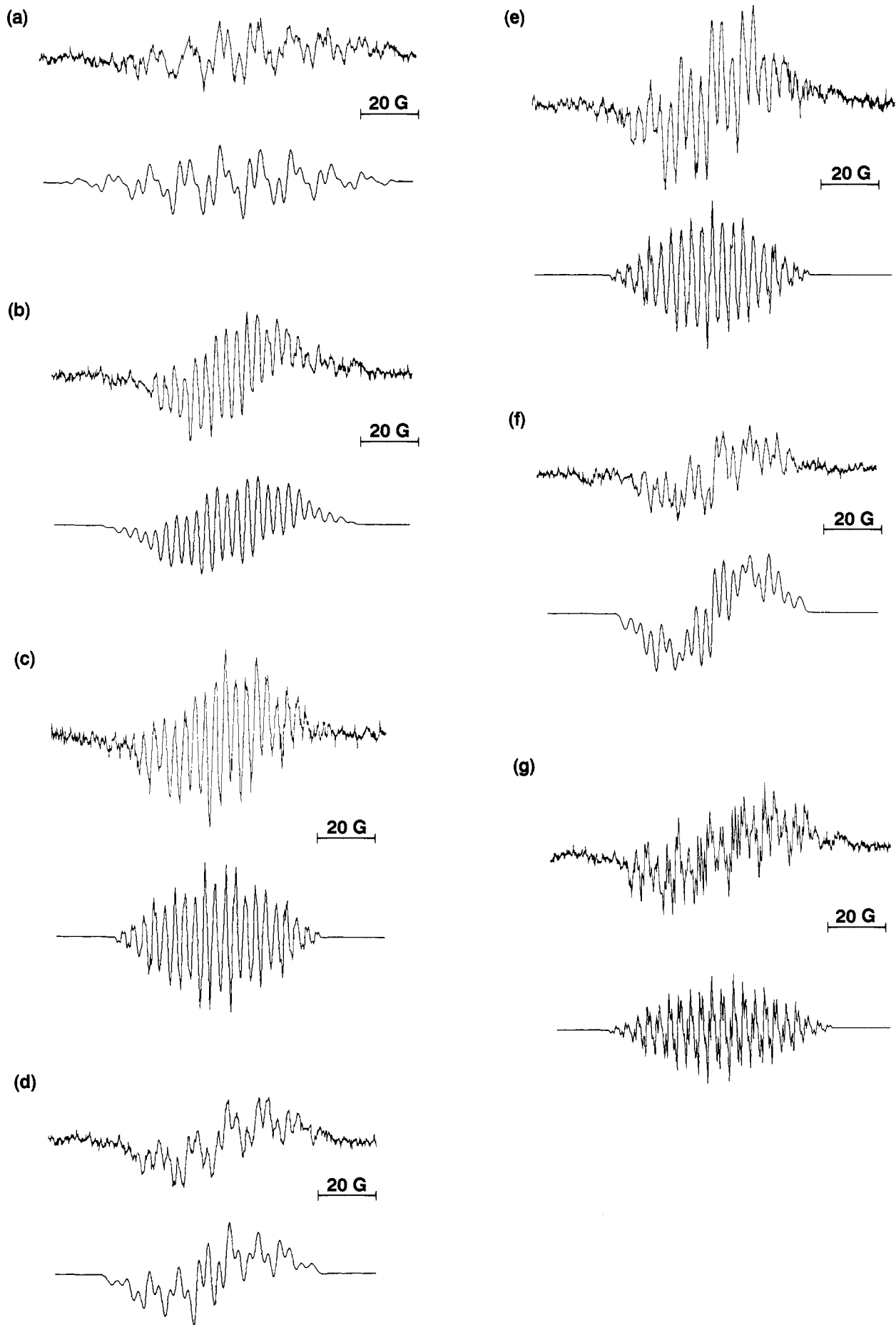
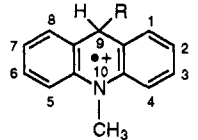


Figure 2. ESR spectra of AcrHR²⁺ and the computer simulation spectra: (a) AcrH₂²⁺, (b) AcrD₂²⁺, (c) AcrHMe²⁺, (d) AcrHEt²⁺, (e) AcrHPr²⁺, (f) AcrHBu²⁺, and (g) AcrHPh²⁺. The hfs values used for the simulation are listed in Table II.

Table II. Hyperfine Splitting (hfs) Values of AcrHR^{•+}


radical cation	hfs, G				
	$a_{\text{H}}^{\text{C-9}}$ (C-9)	$a_{\text{N}}^{\text{N-CH}_3}$ (N-CH ₃)	$a_{\text{H}}^{\text{N-CH}_3}$ (N-CH ₃)	$a_{\text{H}}^{\text{C-2,7}}$ (C-2,7)	$a_{\text{H}}^{\text{C-4,5}}$ (C-4,5)
AcrH ₂ ^{•+}	24.2 (22.4, 19.7) ^a	14.0 (15.4) ^a	10.4 (9.1) ^a	3.4 (-2.4) ^a	1.0 (-1.4) ^a
AcrD ₂ ^{•+}	3.7 ^b	14.0	10.4	3.4	1.0
AcrH ₂ -CD ₃ ^{•+}	24.2	14.0	2.2 ^b	3.4	1.0
AcrHMe ^{•+}	17.8	10.1	7.4	3.4	1.0
AcrHEt ^{•+}	16.9	10.1	7.3	3.4	1.0
AcrHPr ^{•+}	14.4	10.3	7.5	3.4	1.0
AcrHBu ^{•+}	12.0	9.1	6.7	3.4	1.0
AcrHPh ^{•+}	22.3	10.7	7.5	3.3	1.0

^a The values in parentheses are those calculated by the PM3 method.

^b Deuterium splitting value.

C(9) position also causes the change in the splitting pattern as shown in Figure 2c-g.

The observed ESR spectra in parts a-g in Figure 2 can be simulated with the parameters listed in Table II. The hyperfine splitting (hfs) values of AcrH₂-CD₃^{•+} in which three hydrogen atoms at the N-CH₃ position of AcrH₂ are replaced by deuterium are also given in Table II. The assignments in Table II are ensured by comparing the hyperfine splitting (hfs) values of $a_{\text{H}}^{\text{C-9}}$, $a_{\text{D}}^{\text{C-9}}$, $a_{\text{H}}^{\text{N-CH}_3}$, and $a_{\text{D}}^{\text{N-CD}_3}$, since the hfs values of 24.2 and 10.4 G due to C-9 and N-CH₃ protons of AcrH₂^{•+} are decreased by the factor of the magnetogyric ratio of proton to deuterium (0.153) to 3.7 and 2.2 G due to C-9 and N-CD₃ deuterons of AcrD₂^{•+} and AcrH₂-CD₃^{•+}, respectively, when the other hfs values remain identical.²⁵ An important point to note from the results in Table II is the significant decrease in the $a_{\text{H}}^{\text{C-9}}$ values by introducing the substituent at the C-9 position; 24.2 G (AcrH₂^{•+}) > 22.3 G (AcrHPh^{•+}) > 17.8 G (AcrHMe^{•+}) > 16.9 G (AcrHEt^{•+}) > 14.4 G (AcrHPr^{•+}) > 12.0 G (AcrHBu^{•+}). Such change in the $a_{\text{H}}^{\text{C-9}}$ values is predicted by the molecular orbital calculations using the PM3 method (*vide infra*).²¹⁻²³

The hfs values of AcrH₂^{•+} are estimated from the spin densities calculated by the PM3 method.²⁶ The calculated values shown in parentheses in Table II agree reasonably well with the experimental values determined from the ESR spectra in Figure 2 (parts a and b). The optimized structures and the calculated $a_{\text{H}}^{\text{C-9}}$ values of AcrHR^{•+} (R = H, Ph, Prⁱ, and Bu^t) are shown in Figure 3, together with the experimental a_{H} values in Table II for comparison. The acridine ring of AcrHR^{•+} is not planar and the R group at the C-9 position is in a boat-axial conformation.²⁷ In such a case the hfs value of the axial C-9 proton ($a_{\text{H}_{\text{ax}}} = 22.4$ G) is not equivalent to that of the equatorial C-9 proton ($a_{\text{H}_{\text{eq}}} = 19.7$ G). In the ESR spectrum of AcrH₂^{•+}, however, the two C-9 protons are equivalent, $a_{\text{H}}^{\text{C-9}} = 24.2$ G, which agrees reasonably well with the average value (21.1 G) of $a_{\text{H}_{\text{ax}}}$ and $a_{\text{H}_{\text{eq}}}$. Thus, the inversion of the boat structure may occur rapidly in solution in the ESR time scale. As seen in Figure 3, the degree of nonplanarity of AcrHR^{•+} increases with an increase in the folding angle between the planes of the two benzene rings,

(25) Improved resolution obtained in this study results in somewhat different hfs values from those reported in ref 11.

(26) The hfs values of $a_{\text{H}}^{\text{C-9}}$, $a_{\text{N}}^{\text{N-CH}_3}$, and $a_{\text{H}}^{\text{N-CH}_3}$ were evaluated from the 2s spin densities of AcrHR^{•+} calculated by the PM3 method with the UHF formalism. The hfs values of aromatic protons, $a_{\text{H}}^{\text{C-2,7}}$ and $a_{\text{H}}^{\text{C-4,5}}$ were estimated from the 2p_z spin densities (ρ_i) calculated with the RHF formalism by using the relation $a_{\text{H}} = -(27 + 12\rho_i)\rho_i$.²⁴

(27) A boat-axial conformation of the σ adduct AcrH[Re(CO)₅] has recently been reported. See: Lehmann, R. E.; Bockman, T. M.; Kochi, J. K. *J. Am. Chem. Soc.* 1990, 112, 458.

when the calculated $a_{\text{H}_{\text{ax}}}$ values decrease in the order R = H (19.7 G) \approx Ph (19.6 G) > Prⁱ (15.5 G) > Bu^t (10.5 G), in agreement with the experimental observation. Thus, the introduction of substituents at the C-9 position causes the increase in the magnitude of nonplanarity of the acridine ring, resulting in the decrease in the spin density at the C-9 equatorial proton.

One-Electron Oxidation Potentials of AcrHR^{•+}. Slow-scan cyclic voltammograms of AcrHR exhibit an anodic wave with a current maximum, but the complementary cathodic peak, as expected for a reversible redox couple, was not seen at the scan rates up to 1 V s⁻¹ because of the instability of AcrHR^{•+}, except for R = Prⁱ, when the quasi-reversible couple could be seen at the slow-scan rates. The irreversible anodic wave becomes reversible by raising the scan rate up to values ranging from 200 to 2000 V s⁻¹ depending on the substituent R. Figure 4 shows representative examples of fast cyclic voltammograms of AcrHR. The slower scan speed becomes sufficient to gain the reversible wave by replacing the C(9)-H hydrogen with alkyl groups. The one-electron oxidation potential E°_{ox} of the AcrHR^{•+}/AcrHR redox couple (vs Ag/0.01 M AgNO₃) can be readily determined as the average of the anodic and cathodic current maxima. The E°_{ox} values of the various AcrHR thus determined are converted to those vs SCE by adding 0.29 V²⁸ and listed in Table III together with the scan speeds at which the reversible waves are obtained.

We have previously estimated the E°_{ox} value of AcrH₂ and 1-benzyl-1,4-dihydronicotinamide (BNAH) in MeCN at 298 K by analyzing the slow-scan irreversible anodic waves based on the Marcus theory of electron transfer¹⁰ as 0.80 and 0.57 V (vs SCE), respectively.^{9,29} The estimated E°_{ox} value of AcrH₂ agrees well with the value (0.81 V) determined directly by the fast cyclic voltammogram (Table III).³⁰ The replacement of the C(9) hydrogen of AcrH₂ with alkyl groups results in an increase in the E°_{ox} value, which is constant at the range 0.84-0.85 V in the case of R = Me, Et, Prⁱ, CH₂Ph, 1-CH₂C₁₀H₇, and CHPh₂. The E°_{ox} value is increased slightly in the case of R = Bu^t (0.86 V) and Ph (0.88 V). A further increase in the E°_{ox} value is noticed in the case of electron withdrawing substituents: R = CH₂COOEt (0.89 V), CMe(H)COOEt (0.92 V), and CMe₂COOEt (0.92 V).

The adiabatic ionization potentials (I_a) in the gas phase can be calculated as the difference in the heat of formation (ΔH_f) between the neutral form with the optimized structure and the optimized radical cation form by using the PM3 method with RHF formalism (see the Experimental Section). The calculated I_a values of AcrHR are also listed in Table III. The large E°_{ox} values in the case of electron-withdrawing substituents (R = CH₂COOEt and CMe(H)COOEt) (0.89 V) are consistent with the large I_a values as compared to those of the other substituents (Table III). However, the replacement of C(9) hydrogen by the alkyl or phenyl group does not necessarily result in an increase in the I_a value in contrast to the apparent increase in the E°_{ox} value. For example, the I_a value in the case of R = Ph (7.38 eV) is slightly smaller than that of AcrH₂ (7.39 eV), while the E°_{ox} value (0.88 V) is significantly larger than that of AcrH₂ (0.81 V). Similarly, the increase of the E°_{ox} value in the case of Bu^t as compared to that of AcrH₂ is not apparent in the corresponding I_a value. Such discrepancy may be attributed to the difference in the solvation energy attendant upon electron-transfer oxidation in MeCN. The Ph and Bu^t groups may result in a decrease in the solvation energy of the corresponding radical cation because of the charge delocalization. Such difference in the solvation

(28) Mann, C. K.; Barnes, K. K. *Electrochemical Reactions in Non-aqueous Systems*; Marcel Dekker: New York, 1970.

(29) Fukuzumi, S.; Hironaka, K.; Nishizawa, N.; Tanaka, T. *Bull. Chem. Soc. Jpn.* 1983, 56, 2220.

(30) Savéant et al.⁸ have also reported the E°_{ox} value of AcrH₂ in MeCN containing 0.60 M Et₄NBF₄ at 293 K by using the fast cyclic voltammetry as 0.86 V (vs SCE), which agrees reasonably well with the value in MeCN containing 0.10 M Bu₄NClO₄ at 298 K determined in this study (Table III) when the difference in the experimental conditions is taken into account.

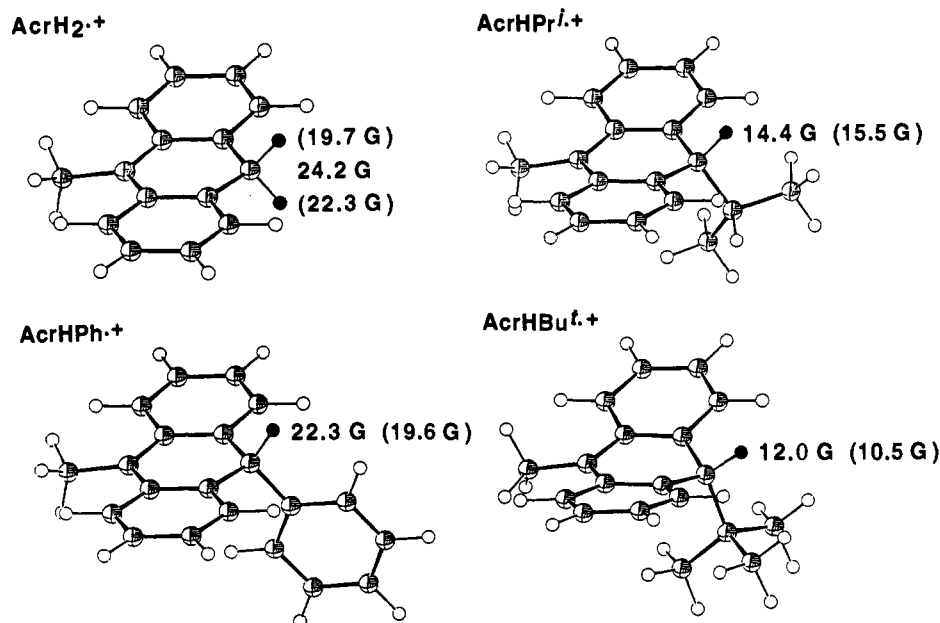


Figure 3. Optimized structures and hfs values of C(9)-H protons of AcrHR⁺⁺ (the values in parentheses are those calculated by the PM3 method).

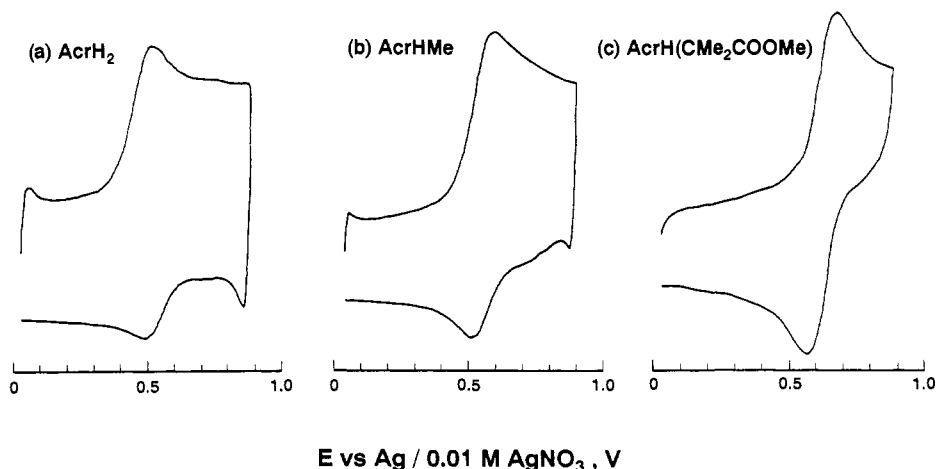


Figure 4. Cyclic voltammograms of (a) AcrH₂ (2000 V s⁻¹), (b) AcrHMe (1000 V s⁻¹), and (c) AcrH(CMe₂COOMe) (200 V s⁻¹) in MeCN containing 0.10 M Bu₄NClO₄ at 298 K.

may be much more enhanced when compared between BNAH⁺⁺ and AcrH₂⁺⁺ containing a monocyclic and tricyclic ring, respectively. The solvation of BNAH⁺⁺ is expected to be significantly larger than that of AcrH₂⁺⁺, resulting in the significant decrease in the E°_{ox} value (0.57 V) as compared to that of AcrH₂ (0.81 V), in contrast to the increase in the I_a value of BNAH (Table III).

Decay Kinetics of AcrHR⁺⁺. A typical example of the decay of AcrHR⁺⁺ (R = Me) is shown in Figure 5. At the initial stage the decay obeys the second-order kinetics as shown in the linear plot of $[\text{AcrHMe}^{++}]^{-1}$ vs time. On the other hand, the decay at the longer time obeys the first-order kinetics as shown in the plot of $\ln(A_0 - A)$ vs time, where A_0 is the initial absorbance at $\lambda_{\text{max}} = 660$ nm due to AcrHMe⁺⁺ and A is the absorbance at the time t . When the deviation from the second-order plot starts, the first-order decay kinetics begins to hold (Figure 5). Thus, the decay kinetics of AcrHR⁺⁺ is given by eq 4, where k_1 and k_2 are

$$-d[\text{AcrHR}^{++}]/dt = k_1[\text{AcrHR}^{++}] + k_2[\text{AcrHR}^{++}]^2 \quad (4)$$

the first-order and the second-order decay rate constants, respectively. The k_1 and k_2 values of AcrHR⁺⁺ obtained from the slopes of the first-order and second-order plots, respectively, are listed in Table IV, together with the absorption maxima of

Table III. Fast Cyclic Voltammetric Data for the One-Electron Oxidation of AcrHR in MeCN Containing 0.10 M Bu₄NClO₄ and the Adiabatic Ionization Potentials (I_a) Calculated by the PM3 Method

AcrHR	sweep rate, V s ⁻¹	$E^{\circ}_{\text{ox}},^a$ V	$I_a,^b$ eV
AcrH ₂	2000	0.81 (0.80) ^c	7.39
AcrD ₂ , R =	2000	0.81	
Me	1000	0.84	7.42
Et	500	0.84	7.37
Pr ⁱ	2	0.84	7.38
CH ₂ Ph	500	0.84	7.38
1-CH ₂ C ₁₀ H ₇	200	0.85	7.43
CHPh ₂	2000	0.84	7.38
Bu ^t	200	0.86	7.40
Ph	1000	0.88	7.38
CH ₂ COOEt	1000	0.89	7.51
CMe(H)COOEt	500	0.92	7.45
CMe ₂ COOMe	200	0.92	7.50
BNAH		(0.57) ^c	7.55

^a Converted to the value vs SCE. The experimental errors are within ± 0.01 V. ^b Calculated from the difference in the heat of formation (ΔH_f) between AcrHR⁺⁺ and AcrHR. ^c Taken from ref 9.

AcrHR⁺⁺. When AcrH₂ is replaced by AcrD₂, the large primary kinetic isotope effects are observed for both the first-order and

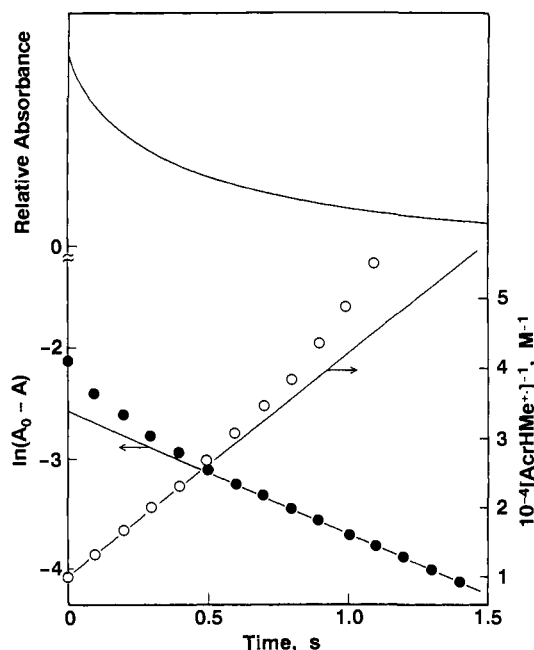


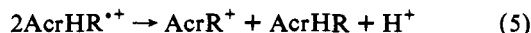
Figure 5. Decay of the absorbance due to AcrHR²⁺ formed in the electron-transfer oxidation of AcrHMe (1.0×10^{-4} M) by [Fe(phen)₃](PF₆)₃ (5.0×10^{-4} M) in deaerated MeCN at 298 K: first-order (●) and second-order (○) plots.

Table IV. First-Order (k_1) and Second-Order (k_2) Rate Constants for the Decay of AcrHR²⁺ and the Absorption Maxima of AcrHR²⁺, Produced in Electron-Transfer Oxidation of AcrHR by [Fe(phen)₃](PF₆)₃ or Fe(ClO₄)₃ in MeCN at 298 K

AcrHR	$k_1,^a$ s ⁻¹	$k_2,^a$ M ⁻¹ s ⁻¹	$\lambda_{\max},$ nm
AcrH ₂	6.4 (3.8) ^b	2.0×10^5 (7.0×10^4) ^b	640
AcrD ₂ , R =			
Ph	7.1 $\times 10^{-1}$	2.0×10^4	640
Me	4.1	1.2×10^5	675
Et	1.1 (8.5×10^{-1}) ^b	3.2×10^4	660
Pr ⁱ		(1.1×10^4) ^b	
Et	4.9×10^{-1}	1.0×10^4	670
CH ₂ COOEt	3.7×10^{-1}	1.1×10^4	670
Pr ⁱ	($\ll 1 \times 10^{-1}$) ^b	<i>c</i>	700
CMe(H)COOEt	$\ll 1 \times 10^{-1}$	<i>c</i>	700
CH ₂ Ph	2.1×10	<i>c</i>	690
1-CH ₂ C ₁₀ H ₇	(1.7×10^2) ^b	<i>c</i>	690
Bu ⁱ	1.4×10 (1.1×10) ^b	<i>c</i>	710
CMe ₂ COOMe	(7.2×10) ^b	<i>c</i>	710

^a Produced in the reaction of AcrHR (1.0×10^{-4} M) and [Fe(phen)₃]³⁺ (5.0×10^{-4} M) unless otherwise noted. The experimental errors are within $\pm 10\%$. ^b Produced in the reaction of AcrHR (1.0×10^{-4} M) and Fe(ClO₄)₃ (1.5×10^{-3} M). ^c Too small to be determined accurately.

second-order decay ($k_H/k_D = 9.0$ and 8.0 , respectively) as shown in Table IV, indicating that both processes involve the transfer of hydrogen nucleus. The second-order decay of AcrHR²⁺ may be ascribed to the disproportionation of AcrHR²⁺ to yield AcrR⁺, AcrHR, and H⁺ (eq 5). Both the k_1 and k_2 values of AcrHR²⁺



decrease by introducing the 9-substituents R in the order R = H > Ph > Me > Et = CH₂COOEt. No second-order decay has been detected for the bulkier substituents R = Prⁱ, CMe(H)-COOEt, CH₂Ph, 1-CH₂C₁₀H₇, Buⁱ, and CMe₂COOMe under the present experimental conditions. In contrast, the large k_1 values are obtained for the first-order decay of AcrHR²⁺ with R = CH₂Ph, 1-CH₂C₁₀H₇, Buⁱ, and CMe₂COOMe, which involve the C(9)-C bond cleavage in the oxidation with Fe³⁺ (eq 2, Table I) as compared with the other substituents (R = H, Me, Et, Ph, and CH₂COOEt) which involve only the C(9)-H bond cleavage (eq 1, Table I). Thus, the first-order decay of AcrHR²⁺ is ascribed

Scheme I

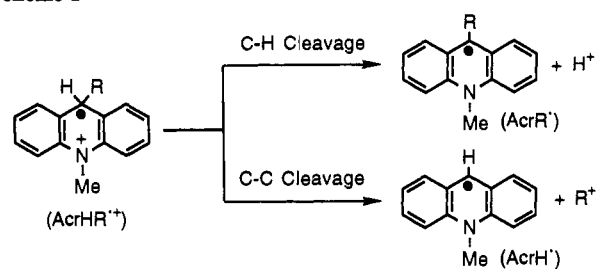
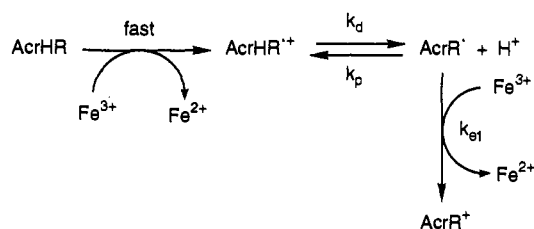


Table V. The C(9)-C and C(9)-H Bond Distances (pm) in AcrHR (d_{C-C} , d_{C-H}) and the Changes in AcrHR²⁺ (Δd_{C-C} , Δd_{C-H}), Calculated by the PM3 Method

AcrHR R =	d_{C-C}	Δd_{C-C}	d_{C-H}	Δd_{C-H}
H			111.1	+0.3
Me	152.7	+0.2	112.0	+0.2
Et	154.1	+0.2	112.0	+0.2
Ph	151.1	-0.2	112.2	+0.3
CH ₂ COOEt	154.0	+0.1	112.0	+0.2
CMe(H)COOEt	155.3	+0.1	112.1	+0.2
CH ₂ Ph	154.7	+0.3	112.1	+0.3
Pr ⁱ	155.2	+0.4	112.2	+0.2
1-CH ₂ C ₁₀ H ₇	154.7	+0.3	112.1	+0.3
CHPh ₂	155.8	+0.5	112.4	+0.6
Bu ⁱ	156.5	+0.5	112.2	+0.1
CMe ₂ COOMe	156.6	+0.2	112.1	+0.2

Scheme II



to the C(9)-H bond cleavage, *i.e.*, the deprotonation and the C(9)-C bond cleavage depending on the substituent R as shown in Scheme I. In the case of R = H, Ph, Me, Et, and CH₂COOEt, the deprotonation of AcrHR²⁺ occurs exclusively, and the deprotonation rate decreases with introduction of the substituent R. As the deprotonation rate is diminished, the C-C bond cleavage starts to occur in the case of R = CH₂Ph, 1-CH₂C₁₀H₇, Buⁱ, and CMe₂COOMe, resulting in the significant increase in the k_1 values. The scan rates of the cyclic voltammograms to gain the reversible anodic wave in Table III may be determined by the change in both the k_1 and k_2 values. The increase in the selectivity for the C-H bond cleavage in the electron-transfer oxidation of AcrHCH₂Ph in the presence of H₂O (Table II) may be ascribed to the enhancement of the deprotonation rate (k_1) because of the favorable solvation of H₂O to proton.

The change in the selectivity for the C-H vs C-C bond cleavage of AcrHR²⁺ is well reflected in the variation of the C-H and C-C bond lengths between AcrHR and AcrHR²⁺ as shown in Table V, where the C-C and C-H bond lengths (d_{C-C} and d_{C-H}) in the optimized structures of AcrHR and the change (Δd_{C-C} and Δd_{C-H}) in AcrHR²⁺, are calculated by the PM3 method.²¹⁻²³ The d_{C-C} value of AcrHR²⁺ increases (Table V) as the selectivity of the C-C bond cleavage increases (Table I). In particular, the d_{C-C} value is the largest (157 pm) for R = Buⁱ and CMe₂COOMe, when the C-C bond is cleaved exclusively. The change in the elongation of the C-H vs C-C bond of AcrHR²⁺ depending on the substituent R may be closely related to the structural change of AcrHR²⁺ in Figure 3, associated with the change in the hfs values of the equatorial protons.

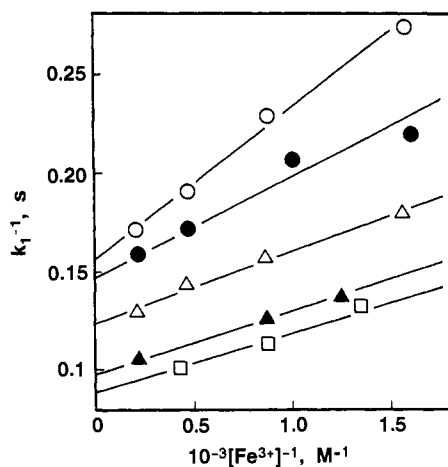


Figure 6. Plots of k_1^{-1} vs $[\text{Fe}^{3+}]^{-1}$ for the decay of AcrH_2^{++} in the presence of HClO_4 in deaerated MeCN at 298 K: $[\text{HClO}_4]$ (70%) = 1.2×10^{-2} M (○), 2.3×10^{-2} M (●), 5.8×10^{-2} M (△), 8.6×10^{-2} M (▲), 1.2×10^{-1} M (□).

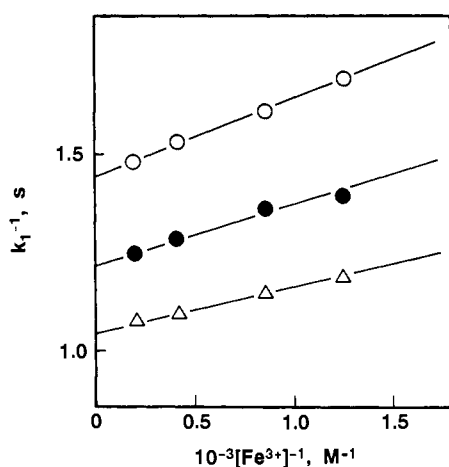


Figure 7. Plots of k_1^{-1} vs $[\text{Fe}^{3+}]^{-1}$ for the decay of AcrHMe^{++} in the presence of HClO_4 in deaerated MeCN at 298 K; $[\text{HClO}_4]$ (70%) = 1.2×10^{-2} M (○), 2.3×10^{-2} M (●), 5.8×10^{-2} M (△).

Determination of the pK_a Values of AcrHR^{++} . The direct determination of the deprotonation rate constants k_1 of AcrHR^{++} may allow us to evaluate the pK_a values of AcrHR^{++} which are fundamental in understanding the oxidation mechanism of NADH analogs. The deprotonation of AcrHR^{++} may be in equilibrium with the protonation of AcrR^* (Scheme II). In the oxidation of AcrHR with Fe^{3+} , the facile electron transfer from AcrR^* to Fe^{3+} (Scheme II) may also occur to yield AcrR^+ , judging from the low oxidation potential of AcrH^* (E°_{ox} vs = -0.43 V)⁹ as compared with that of AcrH_2 (E°_{ox} vs SCE = 0.81 V). According to Scheme II, the observed first-order decay rate constant k_1 is given by eq 6. Equation 6 is rewritten by eq 7, which predicts

$$k_1 = k_{\text{et}} k_d [\text{Fe}^{3+}] / (k_{\text{et}} [\text{Fe}^{3+}] + k_p [\text{H}^+]) \quad (6)$$

$$k_1^{-1} = k_d^{-1} + (k_p [\text{H}^+] / k_d k_{\text{et}}) [\text{Fe}^{3+}]^{-1} \quad (7)$$

a linear correlation between k_1^{-1} and $[\text{Fe}^{3+}]^{-1}$. The validity of eq 7 is confirmed by the linear plot of k_1^{-1} vs $[\text{Fe}^{3+}]^{-1}$ for the first-order decay of AcrH_2^{++} in the presence of various concentrations of HClO_4 as shown in Figure 6. Similar linear plots are obtained for the decay of AcrHMe^{++} as shown in Figure 7. From the intercepts are obtained the deprotonation rate constants k_d . Since the electron transfer from AcrH_2 ($E^{\circ}_{\text{ox}} = 0.81$ V) to Fe^{3+} is too fast to be determined by a stopped-flow technique, the electron transfer from AcrR^* (R = H: $E^{\circ}_{\text{ox}} = -0.43$ V),⁹ which

Table VI. Deprotonation Rate Constants (k_d) and pK_a of AcrH_2^{++} and AcrHMe^{++} in the Presence of HClO_4 in Deaerated MeCN at 298 K

$[\text{HClO}_4]$, M	$k_d(\text{AcrH}_2)^a$, s^{-1}	$pK_a(\text{AcrH}_2)^b$	$k_d(\text{AcrHMe})^a$, s^{-1}	$pK_a(\text{AcrHMe})^b$
1.2×10^{-2}	6.4	8.1	7.0×10^{-1}	8.5
2.3×10^{-2}	6.8	7.6	8.2×10^{-1}	8.1
5.8×10^{-2}	8.2	7.1	9.5×10^{-1}	7.6
8.6×10^{-2}	10.3	6.9		
1.2×10^{-1}	11.5	6.8		

^a The experimental errors are within $\pm 10\%$. ^b The experimental errors are within ± 0.1 .

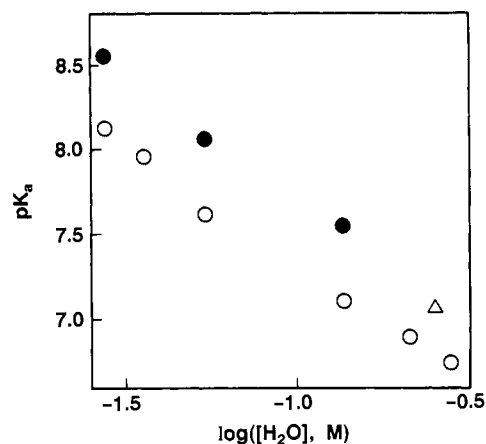


Figure 8. Plots showing the dependence of pK_a of AcrH_2^{++} (○) and AcrHMe^{++} (●) on the H_2O concentration ($\log [\text{H}_2\text{O}]$) of MeCN containing HClO_4 at 298 K. The ratio of $[\text{H}_2\text{O}]/[\text{HClO}_4]$ is 2.4 (○, ●) and 16.7 (△).

is a much stronger one-electron reductant than AcrH_2 , to Fe^{3+} may well be assumed to be diffusion-limited, *i.e.*, $k_{\text{et}} = 2.0 \times 10^{10} \text{ M}^{-1} \text{ s}^{-1}$. Thus, the pK_a [$= -\log(k_d/k_p)$] values are obtained from the intercepts and slopes in Figure 6 and Figure 7 by using eq 7. The k_d and pK_a values of AcrHR^{++} (R = H, Me) are listed in Table VI. The k_d values increase with an increase in the HClO_4 concentration, when the pK_a values decrease. Such change in the k_d and pK_a values may be ascribed to the concentration of H_2O contained in the MeCN solution, since HClO_4 (70%) was used for a safety reason. In fact, the pK_a values of AcrH_2^{++} and AcrHMe^{++} decrease with an increase in the H_2O concentration ($[\text{H}_2\text{O}]/[\text{HClO}_4] = 2.4$) contained in the MeCN solution as shown in Figure 8, where the pK_a value of AcrH_2^{++} in the presence of added H_2O (0.21 M, $[\text{H}_2\text{O}]/[\text{HClO}_4] = 16.7$) is included. Thus, the deprotonation of AcrH_2^{++} is accelerated by the presence of H_2O , while the protonation of AcrH^* is retarded, resulting in the significant decrease in the pK_a values with an increase in the H_2O concentration in MeCN. Such variation of the protonation and deprotonation rates may be ascribed to the strong solvation of H_2O to H^+ as compared to that of MeCN.³¹

We have previously evaluated the proton transfer rate constants from AcrH_2^{++} to various bases by analyzing the kinetic data for electron transfer from AcrH_2 to $[\text{Fe}(\text{bpy})_3]^{3+}$ (bpy = 2,2'-bipyridine) in the presence of various bases in MeCN.⁹ The Bronsted plot of the deprotonation rate constant vs the pK_a of bases in H_2O gave the pK_a value of AcrH_2^{++} as 2.0,⁹ which agrees well with the pK_a values obtained in this study ($pK_a = 6.8 - 8.1$), when the difference in the pK_a values in MeCN and H_2O is taken into account (*e.g.*, the pK_a of pyridine is 12.3 in MeCN, but 5.3 in H_2O).^{26,32} On the other hand, Savéant et al.⁸ have recently estimated the pK_a value of AcrH_2^{++} in MeCN based on the

(31) Sawyer, D. T.; Valentine, J. S. *Acc. Chem. Res.* 1981, 14, 393.

(32) Schlessener, C. J.; Amatore, C.; Kochi, J. K. *J. Am. Chem. Soc.* 1984, 106, 7472.

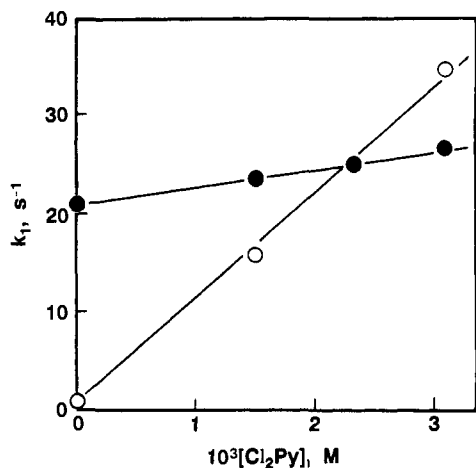


Figure 9. Plots of k_1 vs $[\text{Cl}_2\text{Py}]$ for the decay of $\text{AcrHMe}^{+\cdot}$ (○) and $\text{AcrHCH}_2\text{Ph}^{+\cdot}$ (●) in the presence of 3,5-dichloropyridine (Cl_2Py) in deaerated MeCN at 298 K.

thermochemical analysis as $\text{p}K_a = 0.6$ (or 0.8),³³ which is significantly smaller than the $\text{p}K_a$ values determined directly in this study. The origin of such large discrepancy concerning the $\text{p}K_a$ values is not clear at present. It should be emphasized,

(33) Anne, A.; Hapiot, P.; Moiroux, J.; Neta, P.; Savéant, J.-M. *J. Am. Chem. Soc.* **1992**, *114*, 4694.

however, that the significant effects of H_2O on the $\text{p}K_a$ values in aprotic solvents should be taken into account in determining the $\text{p}K_a$ values in MeCN as clearly demonstrated in Figure 8.

In the case of $\text{AcrHR}^{+\cdot}$ ($\text{R} = \text{CH}_2\text{Ph}$), the first-order decay occurs mainly via the C–C bond cleavage as shown in the large k_1 value as compared with the k_1 values of $\text{AcrHR}^{+\cdot}$ (e.g., $\text{R} = \text{Me}$) which decays via the deprotonation of $\text{AcrHR}^{+\cdot}$ (Scheme I). As such it is difficult to determine the deprotonation rate of $\text{AcrHCH}_2\text{Ph}^{+\cdot}$ in comparison with that of $\text{AcrHMe}^{+\cdot}$. When an external base such as a pyridine derivative is added to the MeCN solution, however, the deprotonation of $\text{AcrHCH}_2\text{Ph}^{+\cdot}$ occurs as shown in Figure 9, where the k_1 values are plotted against the concentration of 3,5-dichloropyridine $[\text{Cl}_2\text{Py}]$ which is added to the system. The k_1 value increases linearly with an increase in $[\text{Cl}_2\text{Py}]$. From the slope of the plot is obtained the rate constant of the proton transfer from $\text{AcrHCH}_2\text{Ph}^{+\cdot}$ to Cl_2Py ($k_H = 1.7 \times 10^3 \text{ M}^{-1} \text{ s}^{-1}$). The large rate constant is obtained for $\text{AcrHMe}^{+\cdot}$ ($k_H = 1.1 \times 10^4 \text{ M}^{-1} \text{ s}^{-1}$). Thus, the reactivity of proton transfer of $\text{AcrCH}_2\text{Ph}^{+\cdot}$ is ten times smaller than that of $\text{AcrHMe}^{+\cdot}$.

Acknowledgment. We are grateful to Professor S. Yanagida for providing us the fast cyclic voltammetry apparatus. We also thank Mr. H. Nakajima for writing the computer program for the ESR simulation. This work was partially supported by a Grant-in-Aid from the Ministry of Education, Science, and Culture, Japan.